Journal of GeoEngineering, Vol. 9, No. 2, pp. 55-73, August 2014
http://dx.doi.org/10.6310/jog.2014.9(2).2

APPLICATION OF AIRBORNE LiDAR TECHNOLOGY IN ANALYZING SEDIMENT-RELATED DISASTERS AND EFFECTIVENESS OF CONSERVATION MANAGEMENT IN SHIHMEN WATERSHED

Cheng-Yang Hsiao [1], Bor-Shiun Lin [2], Chun-Kai Chen [3], and Der-Wen Chang [4]

ABSTRACT

In Taiwan, watershed conservation and management aims to solve problems involving sediment-related disasters. To identify the distribution of sediment sources and the amount of unstable deposit, long-term geomorphologic monitoring has been implemented and countermeasure plans have been progressively executed. LiDAR (Light Detection and Ranging) is a state of the art technology, which is generally used to create the high-precision DEM. airborne and Ground-Based LiDAR have been utilized to precisely scan and measure topological changes. Though, the precision of ground-based LiDAR is higher than airborne, there are limitations to the area that can be scanned in one instance. On the contrary, airborne LiDAR can quickly complete high density scanning to obtain the 3-dimensional data of a target, which can be applied directly to analyzing sediment-related disasters and effectiveness of conservation management in a watershed scale. Taking this into account, this study utilizes multi-period DEMs created by airborne LiDAR and uses ground-based LiDAR to assess DEM accuracy. The DEM is used to estimate amount of sediment trapped within check dams and deposited on hillslopes. Furthermore, the obtained results can be employed as a reference for remediation measures such as dredging and sediment removal when necessary, and for future watershed conservation and management.

Key words: Watershed conservation and management, sediment-related disasters, LiDAR, Shihmen reservoir.

1. INTRODUCTION

Shihmen reservoir began operation in June 1964, providing potable water to agriculture, industry and the public in northern Taiwan. During the flood seasons between 2001 and 2005, Typhoons Toraji, Nari, Aere, Haitang, Matsa, Talim, and Longwang struck Taiwan and triggered serious sediment disasters. Large amounts of sediment were washed into the reservoir, resulting in increased turbidity both in the reservoir and its upstream watershed. Reservoir turbidity increased from normal levels between 30 ~ 50 NTU (Nephelometric Turbidity Units) to between 80,000 ~ 120,000 NTU. This far exceeded the capacity of water treatment plant and lowered its production, triggering water shortage. It had tremendous impact on the daily lives as well as industrial investments. When the NT$80 billion budget (later increased to NT$140 billion) for managing flood problems was approved in 2006, this included the Special Statutes for Remediation of Shihmen reservoir and Its Watershed. Generally, the total sediment yield induced by a typhoon event of reservoir watershed is not entirely delivered to the streams/river. Some unstable sediments remain accumulate and deposit on river beds or along hillslopes. Deposited sediments are then flushed into reservoir region and reduces its storage capacity during the next serious typhoon event. Consequently, the accumulation of event-based sediment material is more problematic to reservoirs in Taiwan than sediment accumulation by long-term erosion. Thus, quantifying the spatial distribution of sediment volume triggered by typhoon events is a very important task for conservation and management of the reservoir. In practical applications, quantifying the sediment volume utilizes geomorphological analysis methods such as ground-based, aerial photogrammetric, laser and radar measurement (Yang 2007). Laser and radar measurement includes Light Detection and Ranging (LiDAR) technology which can provide fast and detailed measurements of the terrain. Sediment transport processes may cause topological changes from a few centimeters to tens of meters. Therefore, utilizing a proper and high-precision measurement tool that detects detailed terrain accurate to the centimeter helps to precisely estimate the amount of sediment trapped within check dams or deposited in hillslope after a rainfall event.

According to Soil and Water Conservation Bureau (SWCB 2009), conservation remediation works are concentrated for larger-scale sediment-related disaster prone area, which are generally termed “priority remediation regions”. The six priority remediation regions were: (1) Yihsing and Junghua (2) Paoliku (3) Sule (4) Shaluntsai (5) Taiping (6) Hsiawenkuang. Their locations are illustrated in Fig. 1 (the period of 2006 measurement did not include Yihsing). The three periods of high-precision DEMs allow us to analyze the terrains’ evolution to study sediment sources, calculate overall sediment productions, and the effectiveness of check dams and slope conservation. They also serve as a reference for the regional prioritization in the next period of conservation and establish a foundation of recycling and sustainability to

Manuscript received November 1, 2013; revised June 24, 2014; accepted July 8, 2014.
[1] Associate Researcher, Disaster Prevention Technology Research Center, Sinotech Engineering Consultants, Taiwan.
[2] Senior Researcher, Disaster Prevention Technology Research Center, Sinotech Engineering Consultants, Taiwan.
[3] Associate Researcher, Disaster Prevention Technology Research Center, Sinotech Engineering Consultants, Taiwan.
[4] Professor (corresponding author), Department of Civil Engineering, Tamkang University, Tamsui, Taiwan (e-mail: dwchang@mail.tku.edu.tw).

extend Shihmen reservoir's service life. This study adopted airborne LiDAR technology which was used to measure the terrain changes in the six priority remediation regions to create high-precision digital elevation model (DEM) in three separate periods (June 2006, August 2008, and November 2008).

2. STUDY AREA

The study area is located in Shihmen watershed, as shown in Fig. 1. Going from north to south, the terrain is long and narrow. In terms of administrative jurisdiction, it contains all of Taoyuan County's Fuxing Township and Hsinchu County's Yufeng Village and Xiuluan Village as well as the northeastern corner of Wufeng Township and the southwestern corner of Yilan County's Datong Township. The watershed's main transportation system relies heavily on mountain roads, and forest roads.

Shihmen watershed is located at 120°10′15″ ~ 121°23′10″ east longitude and 24°25′45″ ~ 24°51′20″ north altitude. Tamsui River's upstream and the Tahan River valley make up its main stream. The watershed area is around 76,352.9 hectares. It borders Taipei County and Yilan County in the east, Taichung County in the south, and Miaoli County in the southwest. Its western portion belongs to Taoyuan County and Hsinchu County. Most of watershed's exposed rocks are sedimentary rocks and mild metamorphic rocks. Its folds and faults are mostly from northeast to southwest. From north to south, the main fold structures are Jinshan Syncline, Jianshi Syncline, Chatienshan Anticline, Sanguang Syncline, Hsuanyuan Syncline, and Chungling Anticline. According to technical regulations for soil and water conservation (SWCB 2006), slopes are divided into seven classes (see Table 1). 53.46% of its slopes are class VI slopes (with gradient between 55% and 100%). There is very little variation in slope aspect. Northward slopes are the most numerous and consist 16.7% while there is very little flatland. Shihmen watershed is located in the Tahan River valley. According to the investigation of debris-flow torrents potential conducted by Soil and Water Conservation Bureau in 2014, Shihmen watershed has 30 potential debris-flow torrents, and most are distributed in the mid-stream and downstream.

The greatest challenge Shihmen reservoir faces today is sedimentation. Whether caused by human development or natural factors, Sediments act as a triggering factor leading to increased turbidity and reduced reservoir storage volume. It also affects the transportation systems, watercourse, and water supply. Sediment source can be classified into four categories (see Fig. 2) and is described below:

a. Surface erosion: Caused by surface runoff and pronounced on bare slopes of soil consisting of fine particles.
b. Landslides and debris flows: Sediment materials from landslide and debris flows in the watershed may be the primary source. Increases in flow cause increased amounts of fine suspended particles to enter the mainstream as well as the reservoir itself.
c. Long-term deposition in riverbed: During storms, settled fine particles become agitated. This is particularly apparent in the upstream check dam area of Shihmen reservoir, which in the past has accumulated large deposits of fine material and is a major source of turbidity.
d. Unstable slope deposits: Fine contents from unstable slope deposits becomes agitated, erode during peak storm flows and are carried by water into the reservoir.

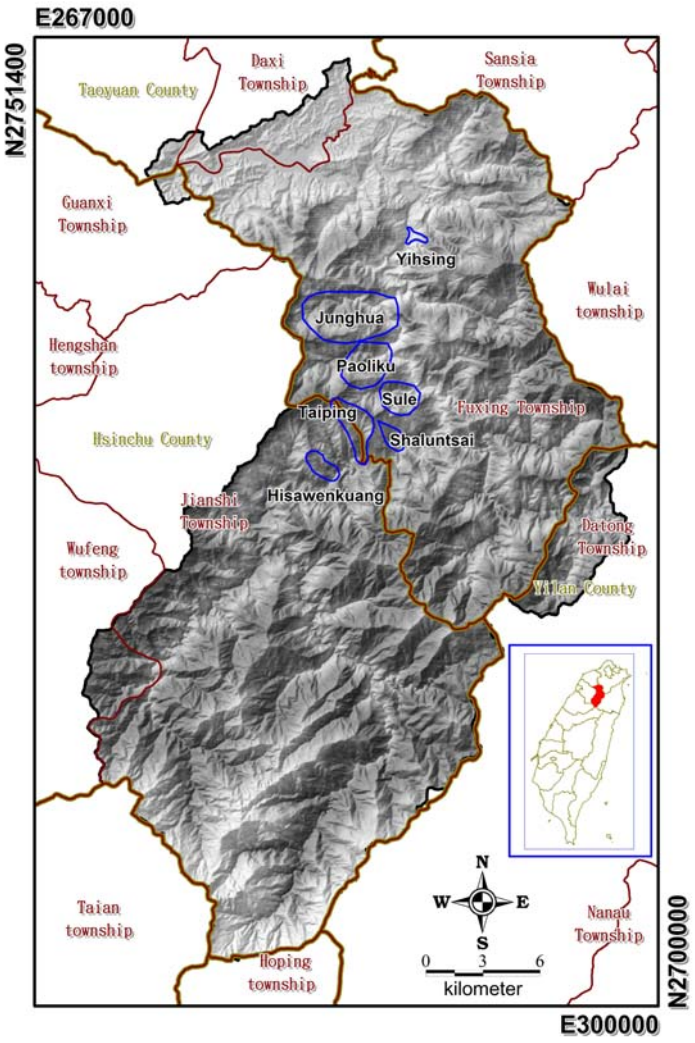

Fig. 1 Locations of the priority remediation regions in Shihmen Watershed

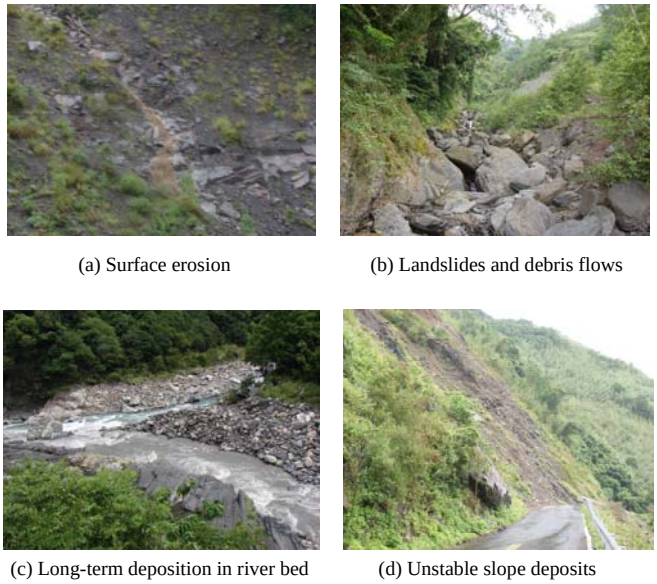

(a) Surface erosion (b) Landslides and debris flows

(c) Long-term deposition in river bed (d) Unstable slope deposits

Fig. 2 Photos of sediment source in Shihmen Watershed

Table 1 Slope classification system (from SWCB 2006)

Class		I	II	III	IV	V	VI	VII
Slope	Percentage (%)	< 5	5 ~ 15	15 ~ 30	30 ~ 40	40 ~ 55	55 ~ 100	≥ 100
	degree (°)	< 2.86	2.86 ~ 8.53	8.53 ~ 16.7	16.7 ~ 21.8	21.8 ~ 28.81	28.81 ~ 45	≥ 45

3. AIRBORNE LiDAR TECHNOLOGY AND DATA PROCESSING OF DEM

Rapid advances in computer science have encouraged improvements in remote sensing techniques. In terms of efficiency and cost, remote sensing is superior to traditional methods especially for collecting and processing data over large areas. Remote sensing has also proven to be very effective in performing rapid, emergency data collection during post disaster recovery periods. As a result, many countries around the world are increasingly exploiting remote sensing to perform prompt, large scale post natural disaster surveys. Jaboyedoff *et al*. (2012) have pointed out that the possibility of acquiring 3D information of the terrain with high accuracy and high spatial resolution is opening up new ways of investigating landslide phenomena, such as interferometric synthetic aperture radar (InSAR) (Tarchi *et al*. 2003) and light detection and ranging (LiDAR) (Sithole and Vosselman 2004; Abellán *et al*. 2009; Evans *et al*. 2009; Sturzenegger and Stead 2009). Particularly, airborne LiDAR is one emerging technology which has been widely applied to watershed sediment monitoring and generate high-resolution point clouds to study terrain evolution. It uses a laser to perform high-density scanning on the target to obtain three dimensional data of topological change. LiDAR sends out multi-impulse wave and receive at most four echoes. Through post-measurement processing, data points such as trees and buildings may be filtered out to obtain the high-precision digital data of the actual terrain. The following is an introduction of airborne LiDAR high-precision measurement, post-measurement processing, quality control, possible advantages, and application.

3.1 Measurement Concepts

LiDAR stands for Light Detection and Ranging. It broadly refers to measuring technology which utilizes a laser to measure its target. Presently, LiDAR uses laser to perform high-density scanning to obtain the three-dimensional data of the target. It is roughly classified into three types: airborne LiDAR, bathymetric LiDAR, and terrestrial LiDAR. Of those, airborne LiDAR using airplanes to conduct surface scanning (airborne laser scanning technology) has been developed the fastest and is the most popular. airborne laser scanning technology originated from NASA research in 1970's and 1980's. The early system could only measure the distance between the airplane and the target and was not suited to produce topographic maps. However, global positioning system (GPS) and inertial navigation system (INS) made high-precision real-time positioning a reality. Recently, the development of airborne laser scanning system is reaching maturity, particularly in establishing high-resolution and high-precision DEM. Through data processing, trees and buildings may be removed entirely to obtain the actual DEM.

In Taiwan, National Cheng Kung University first introduced LiDAR in 2000. In 2002, National Chiao Tung University and Industrial Technology Research Institute (ITRI) collaborated to introduce the commercial system to Taiwan (Shih *et al*. 2002). By 2004, two sets of airborne LiDAR scanning facilities had been brought to Taiwan by the private sector. airborne LiDAR includes Position and Orientation System (POS), Laser Scanner, and System Controller. Of those, POS uses Direct Georeferencing technology and consolidates the 3-D coordinates derived from dynamic GPS positioning technology and data such as the three-axis deflection angles and acceleration measured by Inertial Measurement Unit (IMU) to provide an accurate 200Hz flight-path positioning. Laser Scanner records the projection angles, the differences of reception times, as well as the echoes of the pulse laser at frequencies between 60,000 ~ 150,000Hz. These data are then converted to measured distances and reflection intensities. In addition to being the operating interface, system controller records the time stamps of the above two devices to accurately connect postioning, orientation, as well as other data measured by laser. LiDAR signals are interesting because of their multiple echoes. Up to 4 echoes may be received from a single pulse. Therefore, they can measure the ground surface and the tree tops, even pinpointing the locations of tree trunks or electric lines. This is because LiDAR's laser is conical in shape. The footprint of a single laser beam is a circle with a diameter of 50cm. Parts of it fall on trees and ground. Consequently, it is able to measure the above information from the laser's reflections. airborne LiDAR of measurement concepts is illustrated as Figs. 3 and 4.

3.2 Data Processing

The LiDAR equipment this study used was the airborne laser scanning system ALS50 by German company Leica (see Fig. 5 and Table 2). The primary tasks included preliminary works, measurement and data acquisition, as well as data processing and final check up.

These three steps are described below:

a. Preparation Works

Selecting ground GPS control points is the most important factor in managing measurement from the ground. Principles for ground GPS control point selection are illustrated below:

1. It needs to have excellent openness. Preferably, there is no blocking within 5 degrees of elevation. Disruptions from traffic and wireless base stations should be avoided. Site survey is necessary.
2. It is not necessary to adapt to known points (standard points and satellite control points). Openness should be the priority.
3. Distribution of point locations should allow the vehicle and each GPS control points (at least 2) to be within 30km of each other during aerial scanning.
4. When performing airborne LiDAR scanning, this study considered factors such as terrain elevation, vehicle height, laser scanning angle, flight coverage, flight overlaps, cross flights, point cloud density, and military exercises to draw detailed flight plans. The key points are as follows:
5. Flying Height: The area measured is located in the six priority remediation regions in Shihmen watershed. It is mountainous with great topographic differences(elevation ranges from 354m ~ 1738m, with Taiping River and Paoliku being the highest). Therefore, the initial designed height was 2,400m (8,000ft) and with north-south standard routes.

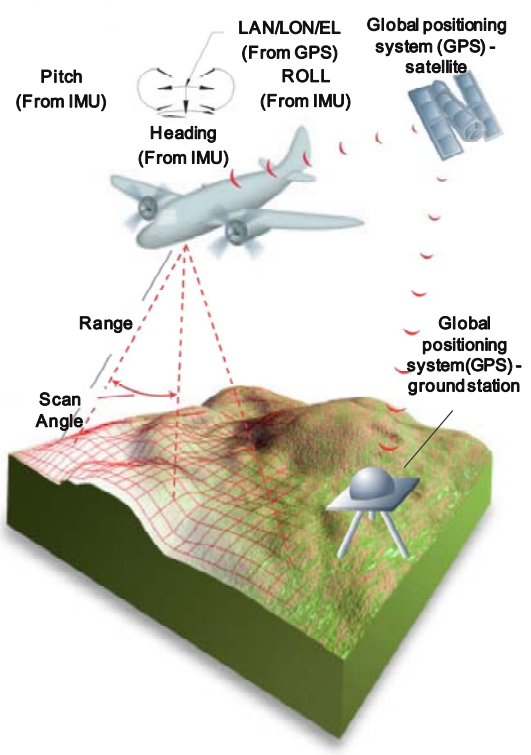

Fig. 3 Conceptual diagram of airborne LiDAR measurement (after Leica Geosystems 2003)

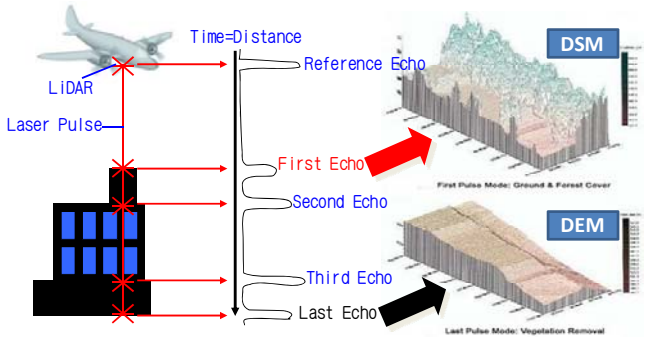

Fig. 4 Schematic layouts of multiple echoes of airborne LiDAR

Fig. 5 Leica ALS50 and Rollei AIC (after Soil and Water Conservation Bureau, 2009)

Table 2 Specification of airborne LiDAR sytem in this study

Item	Description
Scan type	Oscillating, Mirror, Z-shaped
Max. pulse rate	52kHz
Max. scan rate	70Hz
Max. fields of view (Max. FOVs)	75°
Functions at flying heights (AGL)	500 to 4000 m
GPS/IMU	Novatel (2Hz) / Applanix POS AV 510 (200Hz)
Digital camera	Rollei AIC 4080 × 5440 pixels, 9μm / pixel 50mm metric lens
Scanner	0.37m (W) × 0.56m (L) × 0.24m (H), 30 kg
Equipment rack	0.48m (W) × 0.52m (L) × 0.64m (H), 64 kg
Power	28V / 35Amps

6. Laser Measurement Point Density: The average density of the original measurement point should be higher than 1.0 point per square meter.
7. Flight Overlap Proportion: The average flight overlap proportion was designed to be 50%. The actual overlap proportion ranged between 20% ~ 70%.
8. Each flight should have at least two GPS bases receiving GPS measurements. The distances between the bases and the flight path should be less than 30 km.
9. Cross Flight Data: Cross aerial scanning should be conducted at the beginning and the end of the flight. Further, LiDAR system was caliberated at the factory and then periodically recaliberated after being installed on the airplane according to ground control data. Leica ALS50, the model that this study used, needs to be recaliberated every year.

b. Measurement

When conducting aerial scanning, weather conditions should be fully mastered. The necessary hardware check-ups, parameter confirmation, and complete log should be conducted prior to and during measurement based on the flight plan's parameters and quality control protocol.

c. Data Processing

In order to obtain track solutions, GPS information from ground bases and from the flying vehicle as well as IMU inertial navigation data should first be confirmed. After initial assurance of the data's reception quality, dynamic differential solution is obtained. Once the deviation between positive and negative solutions is found to be within 20cm, time series flight path coordinates can be produced. The tracking data obtained are consolidated with original LiDAR scanning data including distance of scanning echoes, scanning angle, signal intensity, order of echoes, and time and equipment calibration parameters. Leica's point cloud conversion software can be used to calculate the 3-dimensional coordinates and intensities under each scanning echo signal's TWD97 coordinate system to get the original point cloud data which saved as in LAS file.

Leica ALS50 airborne LiDAR workflow overview is illustrated in Fig. 6. The original LiDAR point cloud data should be corrected upon their synthesis. However, these data may still contain inaccuracies when conducting data accuracy analysis in the overlapping regions, including Heading, Pitch, Roll, Dz, *etc*. This study used software such as TerraMatch's Find Match function to perform strip adjustment for the entire region so the data can be consistent. After adjustment, software such as TerraScan was used to classify the various point cloud data. The point clouds were segmented into 1km × 1km units to avoid computer overload. TerraScan was then used to filter ground points and editing to extract the ground points from point cloud data as illustrated in Fig. 7. Software such as SCOP++ was used to perform 5m DEM interpolation on surface topography point cloud data. The results of batch processing were integrated into DEM for the entire region. This was then converted to orthometric height by geoid computation and output as multi-period high-precision DEMs of studied areas as shown in Fig. 8.

Presently, LiDAR is superior in resolution, accuracy, convenience, and the ability to remove buildings and trees. Figure 9 illustrates using measurement by aerial photography and airborne LiDAR scanning technology at the confluence of the Tahan river and its tributaries in Shihmen reservoir to establish DEMs. According to the Fig. 9, the DEMs by airborne LiDAR clearly determined detailed terrain information such as torrents and gullies. Schenk (2001) confirmed that elevation accuracy is superior to that of surface positioning. Other related research include detecting height of trees in various categories, forest terrain model creation, sediment yield assessment, terrain evolution, and extraction of building shapes by airborne LiDAR (Avian M. *et al*. 2009; Lin 2010; Hsiao *et al*. 2011; Lin *et al*. 2012a, 2012b, 2013).

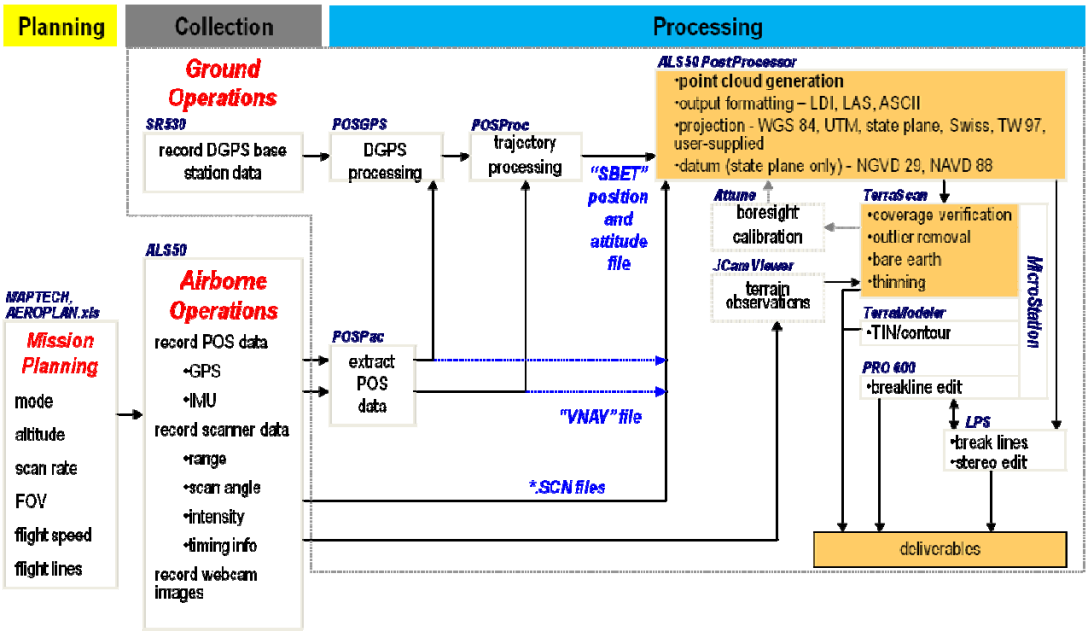

Fig. 6 Leica ALS50 — LiDAR workflow overview (from Leica 2004)

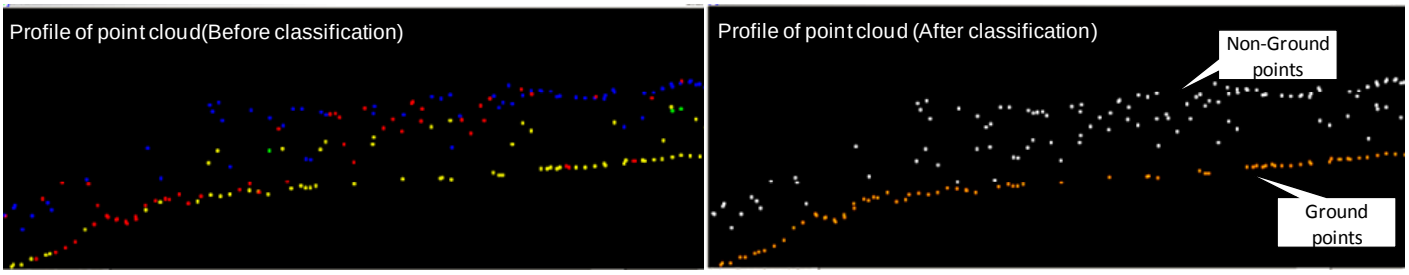

Fig. 7 Classification before and after point clouds

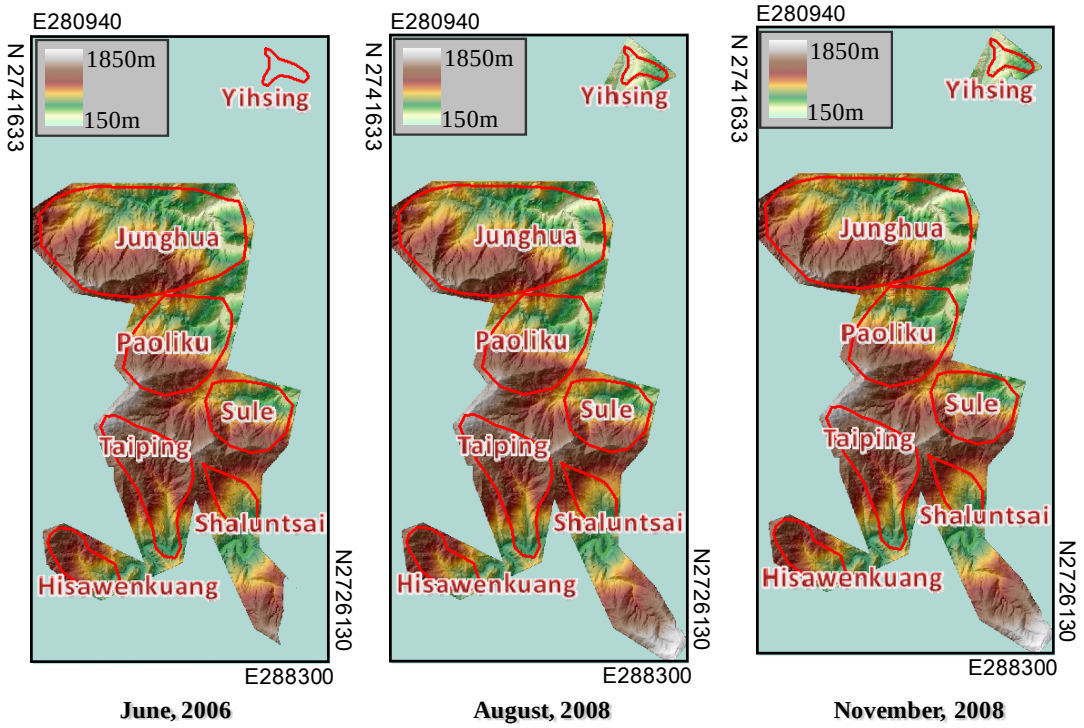

Fig. 8 Multi-period DEMs created by airborne LiDAR

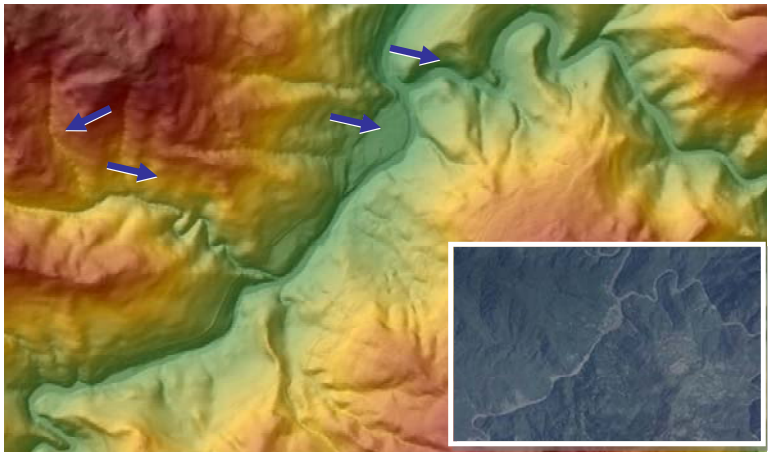

(a) DEM created by aerial Photography

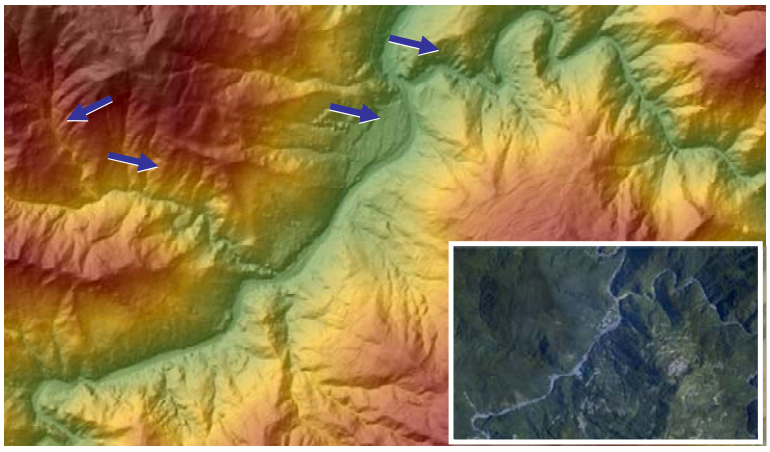

(b) DEM created by airborne LiDAR

Fig. 9 Comparison of DEMs between airborne LiDAR and aerial photography

4. ASSESSMENT ON AIRBORNE LiDAR DEM ACCURACY

Application of airborne LiDAR and its DEMs accuracy are very important to geomorphological evolution assessment. Both prior and later DEM data were used to study terrain evolution. Multiplying DEM elevation difference to the area of the changed region gives the changed volume that indicates this transformation. Further, the accuracy of DEM data needs to be understood to determine whether the difference was due to topographic difference or error. For instance, data from airborne LiDAR were compared to ground-based LiDAR data. If the difference was within 0.5 m, the prior and later elevations of failures should also be compared. If their difference was also within 0.5 m, it may be an error and should not be recommended for earthwork estimate and analysis. In addition, the error in each measurement is different and for comparing with different periods DEMs, self-precision DEM and their mutual error propagation must both carefully considered so as to ensure reliable range of subtracted results from DEMs (Croke *et al*. 2013). Assuming that two DEM has the same precision of 0.5 m, the error based on error propagation theory can be computed by

$$\text{error} = \pm\sqrt{0.5^2 + 0.5^2} = \pm 0.71\text{m} \quad (1)$$

The common measuring techniques used to create DEM are listed in Table 3. According to the table, aerial photography and satellite imaging were used to create DEM, which was compared against ground-based LiDAR from different slopes to estimate the elevation difference formula (Sinotech Engineering Consultants 2006), and ground-based LiDAR had the best spatial resolution and accuracy.

Table 3 Information of common DEM creation techniques

Measuring techniques	airborne LiDAR	Aerial photography	Satellite imaging	Ground-based LiDAR
Resolution	0.5 m ~ 2 m	Resolution：0.10 m ~ 0.50 m (based on mid-sized camera)	Depending on the satellite; multi-spectral imaging is the most widely used among commercial satellites 0.61 m (Quick Bird)	10 mm
Horizontal accuracy	H = ± 0.3 m ~ 0.8 m (depending on the equipment)	Accuracy：± 0.10 m ~ 0.50 m (~ 1 pixel) (based on mid-sized camera)	Depending on the satellite	H = ± 5 cm (depending on the equipment)
Elevation accuracy	V = ± 0.1 m ~ 0.3 m	–	–	V = 0.02 m
Post-processing accuracy	Spatial resolution 5 m	Spatial resolution 50 cm	Before 2003，SPOT-1 ~ SPOT-4 incorporated spatial resolution of 10 m In 2003, SPOT-5 incorporated spatial resolution of 2.5 m In 2004, FORMOSAT-2 incorporated spatial resolution of 2 m	Spatial resolution 10 cm
Steepness and error formula (Using ground-based LiDAR as basis)	$y = 0.0474e^{0.0407x}$ ** *x*: steepness (degree) *y*: elevation difference (m)	$Y = 0.2188e^{0.0499x}$ * *x*: steepness (degree) *y*: elevation difference (m)	$y = 0.678le^{0.0446x}$ * *x*: steepness (degree) *y*: elevation difference (m)	Assessment standards
Scanning range	Scanning width approximately 0.6 km	Depending on the altitude, scale, and overlap ratio	Scene width SPOT-1~SPOT-5 : 60 km FORMOSAT-2 : 24 km	Scanning device is at the center of the circle. Horizontal maximum distance : 2.5 km Horizontal:360 degrees Vertical: + 135degrees ~ 60 degrees
Common application	Design flight path monitoring and terrain illustration; used by this study to perform comprehensive high-precision terrain changes	Design flight path monitoring; generally used in creating city maps	Periodic scanning to meet geologic, geographic, agricultural, hydrological, weather, fishery, and environmental needs; often used in failure determination	Monitoring local key regions; creating building models; often used in measuring failure volumes at river confluences and slopes

* The slope-related empirical formula is referred to Sinotech Engineering Consultants (2006).

** The slope-related empirical formula is obtained from this study.

Airborne LiDAR is indeed superior to ground-based LiDAR in conducting high-precision measurements of topographic changes in the vast Shihmen reservoir. However, for topographic measurements of known, specific small regions, ground-based LiDAR is superior in accuracy, mobility, and cost. It may be possible to conduct annual or biannual measurements by airborne LiDAR over large areas in Shihmen watershed. Periodic monitoring by ground-based LiDAR may be used to verify airborne LiDAR accuracy and renew the high-precision DEM. Accordingly, this study used ground-based LiDAR data to examine the accuracy of airborne LiDAR and to establish a slope-related empirical formula. The instrument specifications of ground-based are listed in Table 4 and its photos as shown in Fig. 10. The following describes how to use the second-period airborne LiDAR data to perform accuracy examination. The comparative area was in Shaluntsai region (see Figs. 11 and 12). The scan distance is not over 150m so that its error is expected to be under 2.3cm (error equation refered to Table 4). Point cloud data were gathered from two section lines as shown in Fig. 13. Green color denotes ground points of airborne LiDAR, and blue color denotes the ground- based LiDAR points. After several examinations of the elevation cross sections, elevations were found to be close in value. Because ground-based LiDAR only had one signal echo from the vegetated regions, it could not obtain the ground point data underneath the vegetation, and discrepancy was possible. After filtering out the vegetated regions, Table 5 was created to show the volume and steepness differences between airborne LiDAR and ground-based LiDAR. The average elevation differences among the different slopes range between 6.32cm to 51.58cm and increase as the steepness increases (see Fig. 14). The average error was 20.24cm. Therefore, it is sufficiently accurate to assess remediation effectiveness. Following is an empirical formula to find error budget between ground-based LiDAR and airborne LiDAR:

$$y = 0.0474\, e^{0.0407x} \tag{2}$$

where x is slope angle (degree); y is difference of elevation (m).

The above equation can be used to calibrate error of DEMs created by both of them.

5. EVALUATION OF THE CONSERVATION MANAGEMENT

Soil and Water Conservation Bureau (2009, 2010) targeted these watersheds and conducted three comprehensive airborne LiDAR scans to create multi-period high-precision DEMs (see Table 6). These measurements can be divided into two duration. The first is between June 2006 ~ August 2008, with Typhoons Sepat, Wipha, Krosa, and Fungwong. The second is between August 2008 ~ November 2008, with Typhoons Nuri, Sinlaku, and Jiangmi. The accumulated rainfall of Typhoon Sinlaku was especially high, reaching up to 914.6mm. Prior high-precision DEM is subtracted from later high-precision DEM. Therefore, the effectiveness of check dams can be assessed by analysing the differences between terrain elevations. A negative value in the grid represents failure or erosion, and positive value indicates deposits. Topological change in a grid can be obtained by multiplying this value by the area of the unit grid (Fig. 15). Further,

Table 4 Specification of ground-based LiDAR system in this study

Item	Description
Maximum distance to be measured	< 2500m
Scan rate per sec	4 points
Horizontal scan angle	± 180°
Vertical scan angle	+ 135° to –60°
Error	20mm ± 20ppm × distance (mm)

Table 5 Elevation and height difference between airborne LiDAR and ground-based LiDAR with respect to slope angle

Slope angle x (°)	Average height difference (cm)	Average volume difference (m^3)
$x < 10°$	6.32	1.58
$10° \le x < 20°$	8.68	2.17
$20° \le x < 30°$	15.45	3.86
$30° \le x < 40°$	20.42	5.1
$40° \le x < 50°$	29.32	7.33
$50° \le x < 60°$	43.18	10.8
$60° \le x < 70°$	51.58	12.9
$70° \le x < 80°$	N/A	N/A
$80° \le x < 90°$	N/A	N/A
Overall average difference	20.24	5.06

Note: Overall average difference was derived from the average of all data

Fig. 10 Photos of Dibit LPM-2K

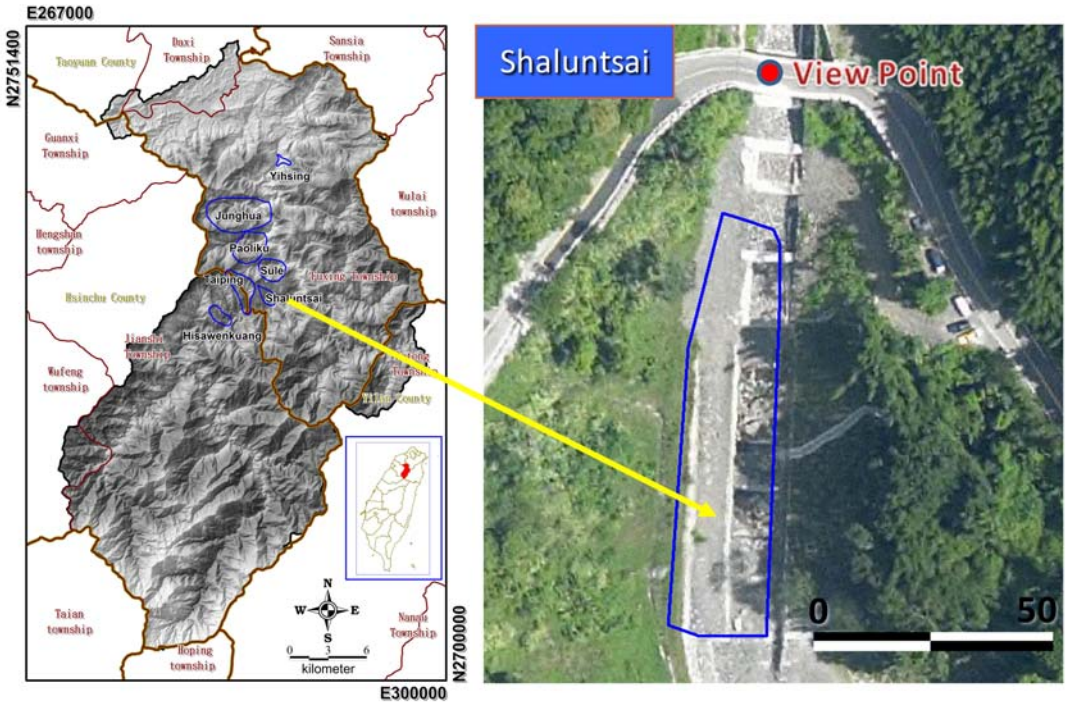

(a) Location of Slaluntsai region (b) Comparative area (blue polygon)

Fig. 11 Comparative area of Slaluntsai region between ground-based LiDAR and airborne LiDAR measurement

(a) Real scene (b) Point cloud

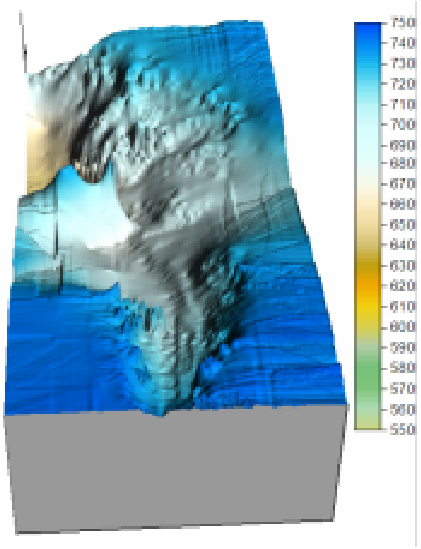

(c) DTM

Fig. 12 Point cloud and DEM created by ground-based LiDAR

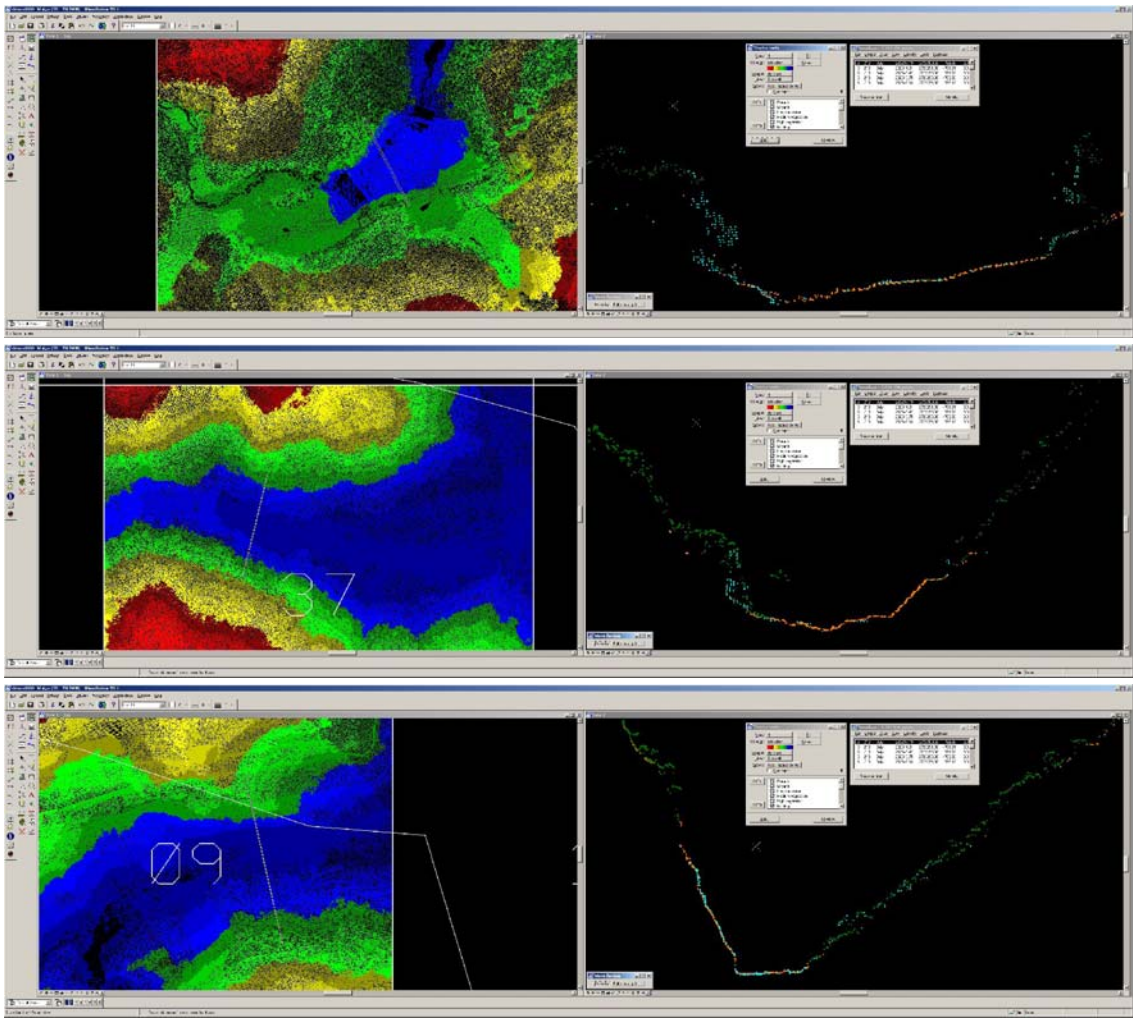

(a) Top view of point cloud (b) Point cloud profile of comparative cross section

Fig. 13 Cross section comparison between airborne LiDAR and ground-based LiDAR

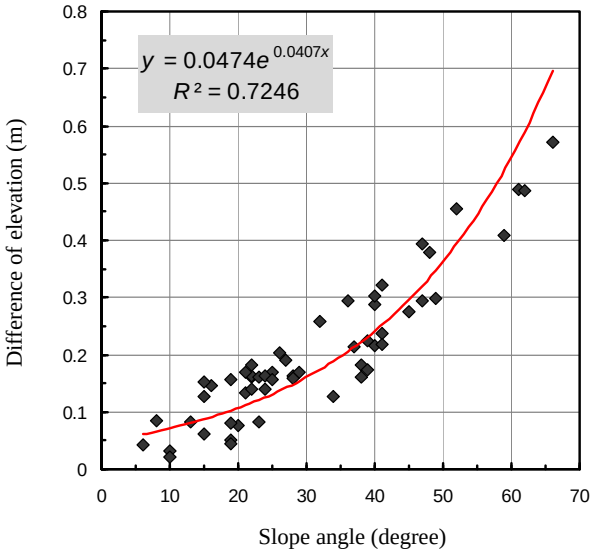

Fig. 14 Relationship between elevation difference and slope angle

Table 6 Airborne LiDAR measurement periods and the relevant typhoons

	Duration	Typhoon events
1	2006.06 (1) ~ 2008.08 (2)	Sepat, Wipha, Krosa, Fungwong
2	2008.08 (2) ~ 2008.11 (3)	Nuri, Sinlaku, Jiangmi

Note 1: The first period of DEM was created in June, 2006 by Soil and Water Conservation Bureau (2006).

Note 2: The second period of DEM was created in August, 2008 by Soil and Water Conservation Bureau (2009).

Note 3: The third period of DEM was created in November, 2008 by Soil and Water Conservation Bureau (2009).

sediment yield is the total volume of terrain changes such as slope failures and river erosions. Sediment trapping rate (STR) can be assessed by measuring the volume of earth in front of the check dams. However, the scanning precision of airborne LiDAR is higher than other measuring technology, but there are still deviations and errors existing in measurement system, GPS and point clouds classification during subtraction of multi-period DEMs. To overcome this problem, some steps of calibrating multi-period DEMs must be implemented initially to eliminate this deviation and error as shown in Fig. 16. Firstly, multi-period DEMs and their corresponding ortho-images for a given region were collected. The largest ortho-image from among these was designated the base map and the Autosync module of Erdas Imagine 9.1 was used to synchronize, align and georeference all of ortho-images with DEM (see Figs. 17, 18). Then, fixed regions on the ortho-images such as roads, sports grounds, helicopter takeoff/landing zones and other regions with few changes were dilineated (see Fig. 19). To calibrate multi-period DEMs, elevation difference of control points for multi-period DEMs in delineated regions were interpolated and equivalent contour lines were drawn. All of the collected DEMs were calibrated on the identical base map according to equivalent contour lines as shown in Fig. 20. Finally, if the precision of calibratied DEMs is under 50cm, they were then applied to analyze sediment-related disasters and evaluate effectiveness of conservation management after interpretation of the landslide area and delineation of river beds (see Fig. 21).

Then, the DEM data sets obtained for each different period by airborne LiDAR could be subtracted from each other to calculate the changes in sediment volume. Since accuracy of the DEM is around 50cm, minute terrain changes may be obtained. In addition to detecting debris flows, landslides, riverbed erosions, and sediment transport, terrain difference between the periods before and after the remediation may also be measured. As mentioned before, the 2006 LiDAR scanning did not include Yihsing region. Therefore, only the two DEM data from 2008 could be studied. Table 7 lists terrain differences for the priority remediation regions. According to the table, between 2006 and August 2008, sediment production was 217,964 m^3. Between August and November 2008, sediment production had been decreasing 87% sediment production (approximately 28,174 m^3) had been decreasing 87% (see Table 7). Although these two phases differed in their hazards and length, the overall management was acceptable in both. This is particularly true for Sule region where sediment production was reduced by 14 times. The following is a description of the topographic and vegetative changes of landslides, streambeds.

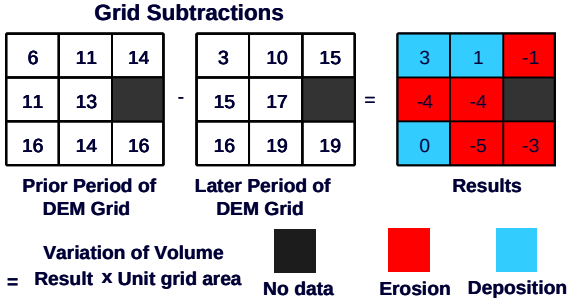

Fig. 15 Grid subtractions between DEM from prior period and later Period (from Hsiao *et al.* 2011)

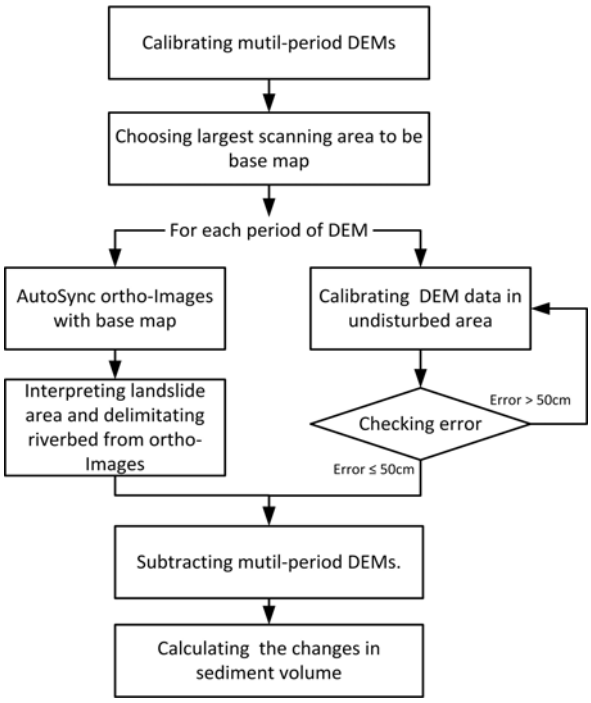

Fig. 16 Procedure of calibrating multi-temporal DEMs

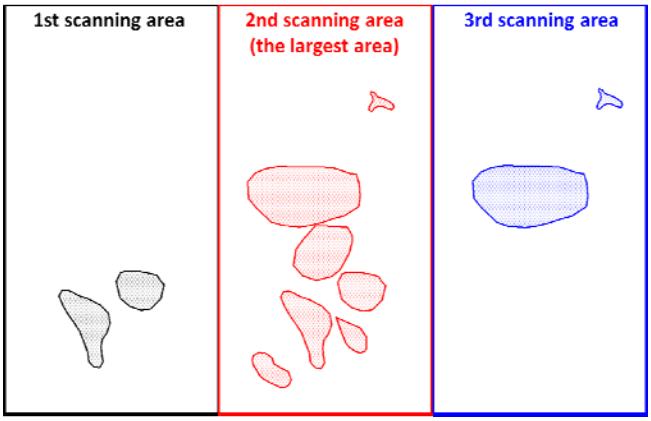

Fig. 17 Determination of base map by the largest scanning area

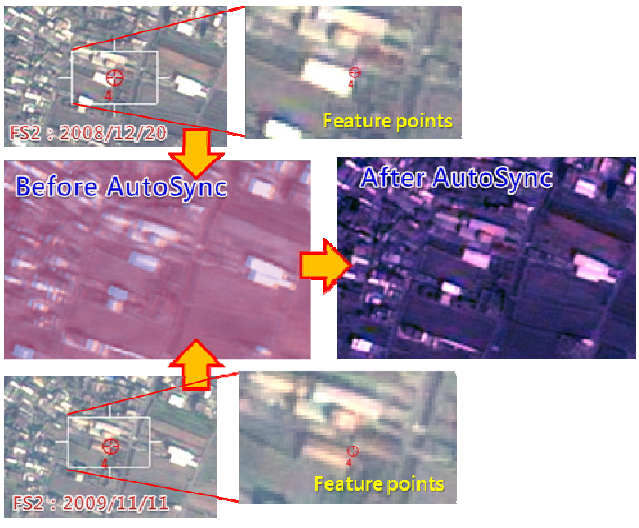

Fig. 18 Schematic layouts of Autosync ortho-images with base map

a. Slope remediation along Taiping region

Figure 22 is a cross section of a large failure along the left bank of the upper section of the Taiping River. Observing the stream bed along the D-D' cross section, the watercourse elevated by 700 m with an average slope of 36 degrees. The result shows that the most severe failure for the area occurred between June 2006 and August 2008. Massive sediment was washed into the river. Vegetation restoration and slope remediation projects completed in 2008 appear to have stabilized the landslide, which did not show signs of expansion afterwards. According to Table 7, sediment yield decreased from 19160.2 m^3 to 3459.8 m^3.

b. Vegetation restoration at Shaluntsai region

Figure 23 is a cross section of a large landslide area on the right bank of Shaluntsai River. Large-scale vegetation restoration was conducted between June 2006 and August 2008. No landslide and debris flows occurred after August 2008, so that the environment of study area has recovered and remained in stable situation after remediation. Sediment yield of each period is listed in Table 7.

c. Effectiveness of check dams at Sule region

Figure 24 shows watercourse change for each period as well as their cross sections. Check dams effectively slowed sediment transport between June 2006 and August 2008. Total sediment trapped in the river channel was 77,271 m^3 from DEM subtractions. The mid-portion of the downstream section of the stream showed clear signs of erosion. New check dams were constructed after August 2008 to the reduce watercourse slope and to stabilize the river bed. After the new check dams were constructed, erosion stopped, and the amount of sediment trapped is 6,285m^3.

Road with split bar

Helicopter take off and landing location

Sports ground

Corner of structure

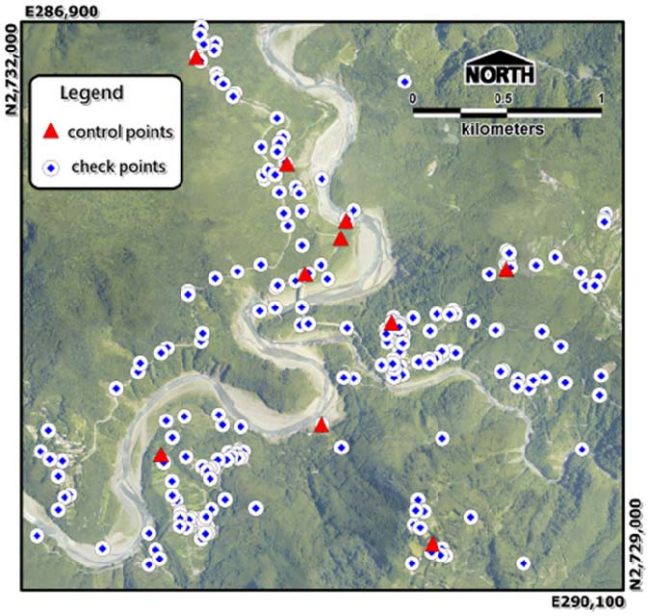

Fig. 19 Control points and check points for calibrating and error checking DEM data

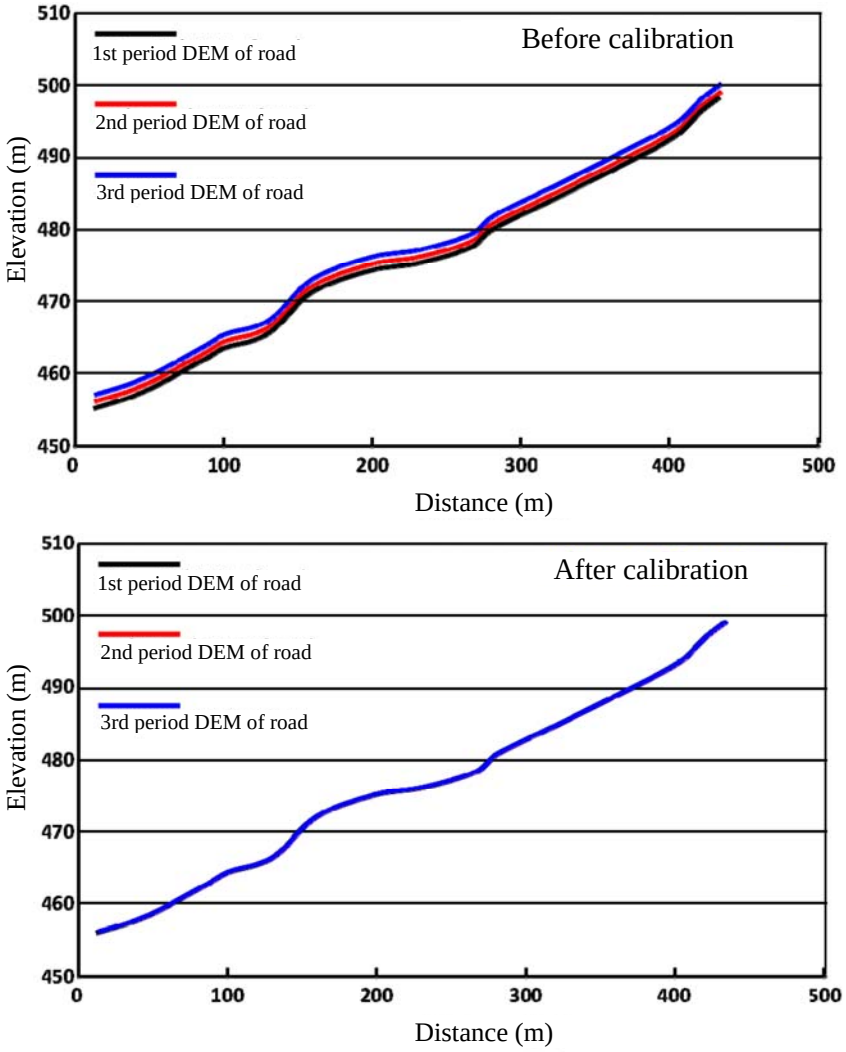

Fig. 20 Before and after calibration for different period DEMs

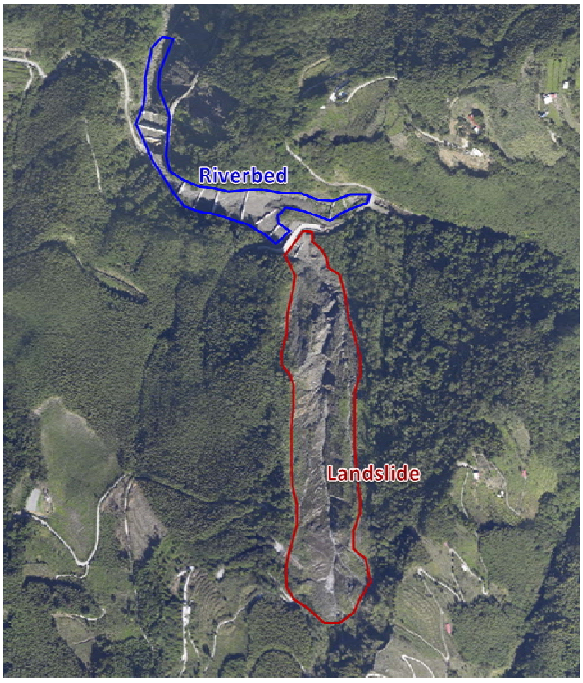

Fig. 21 Interpretation of landslide area and delimitation of river bed from ortho-image

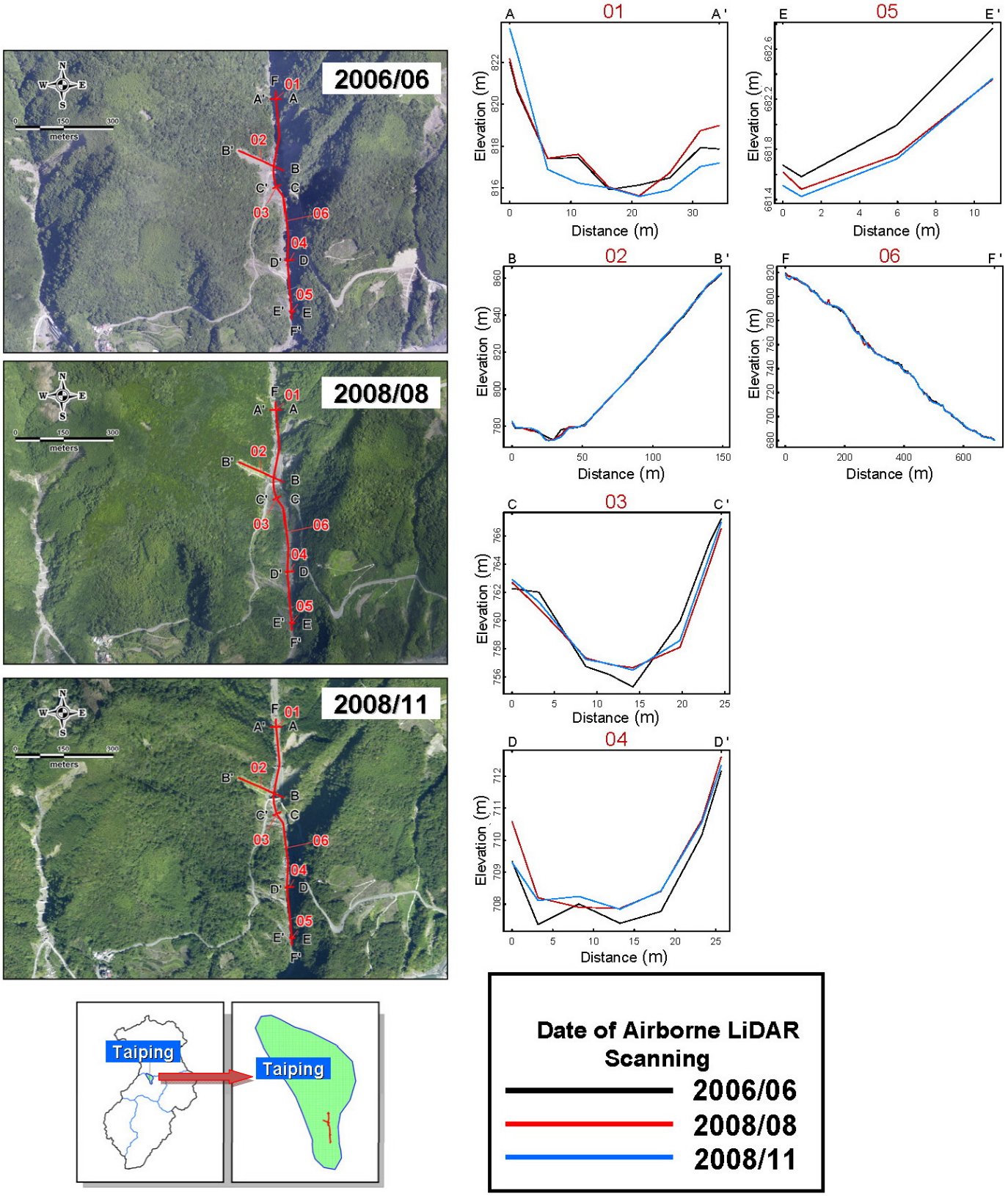

Fig. 22 Cross section analysis of Taiping region

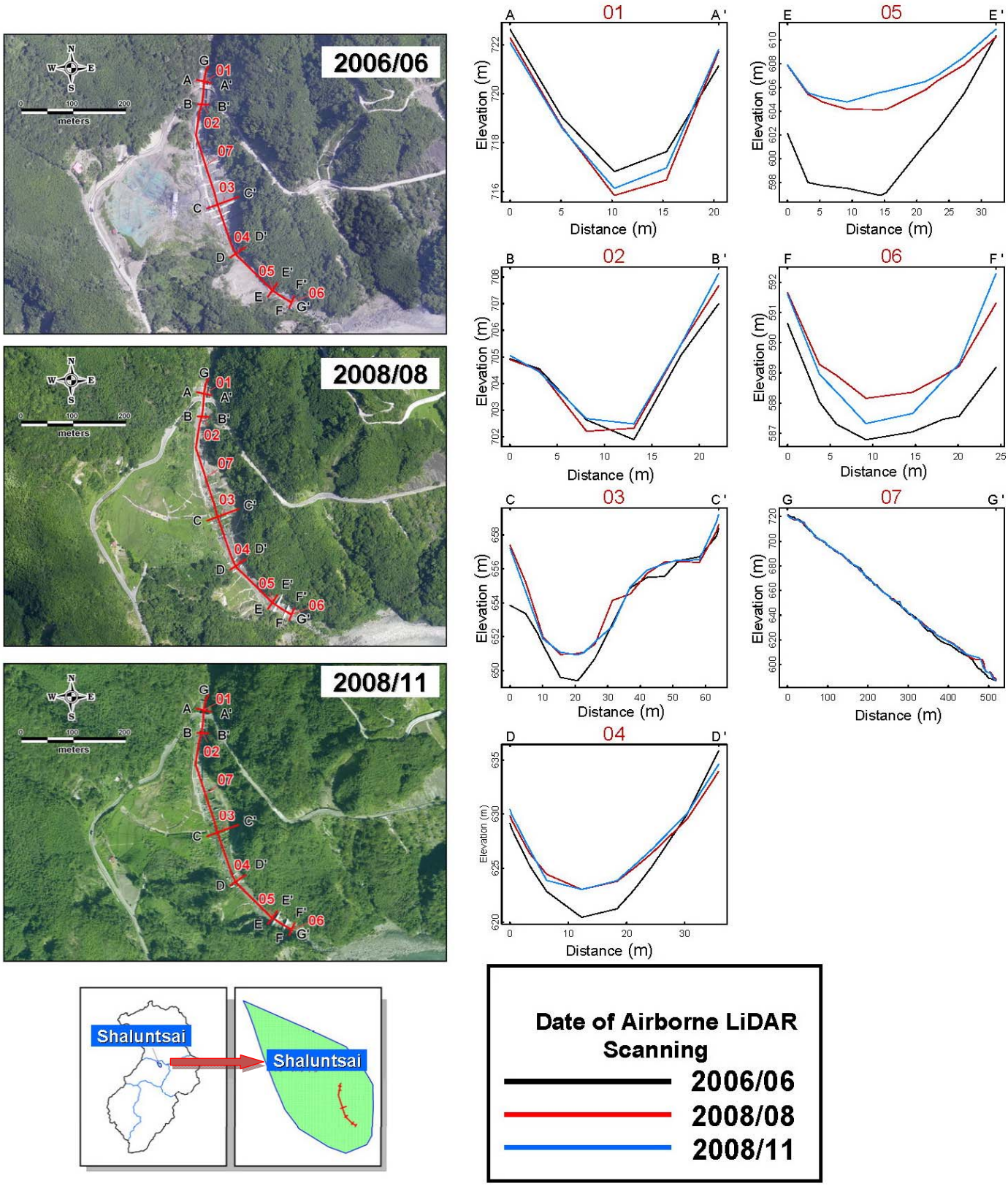

Fig. 23 Cross section analysis of Shaluntsai region

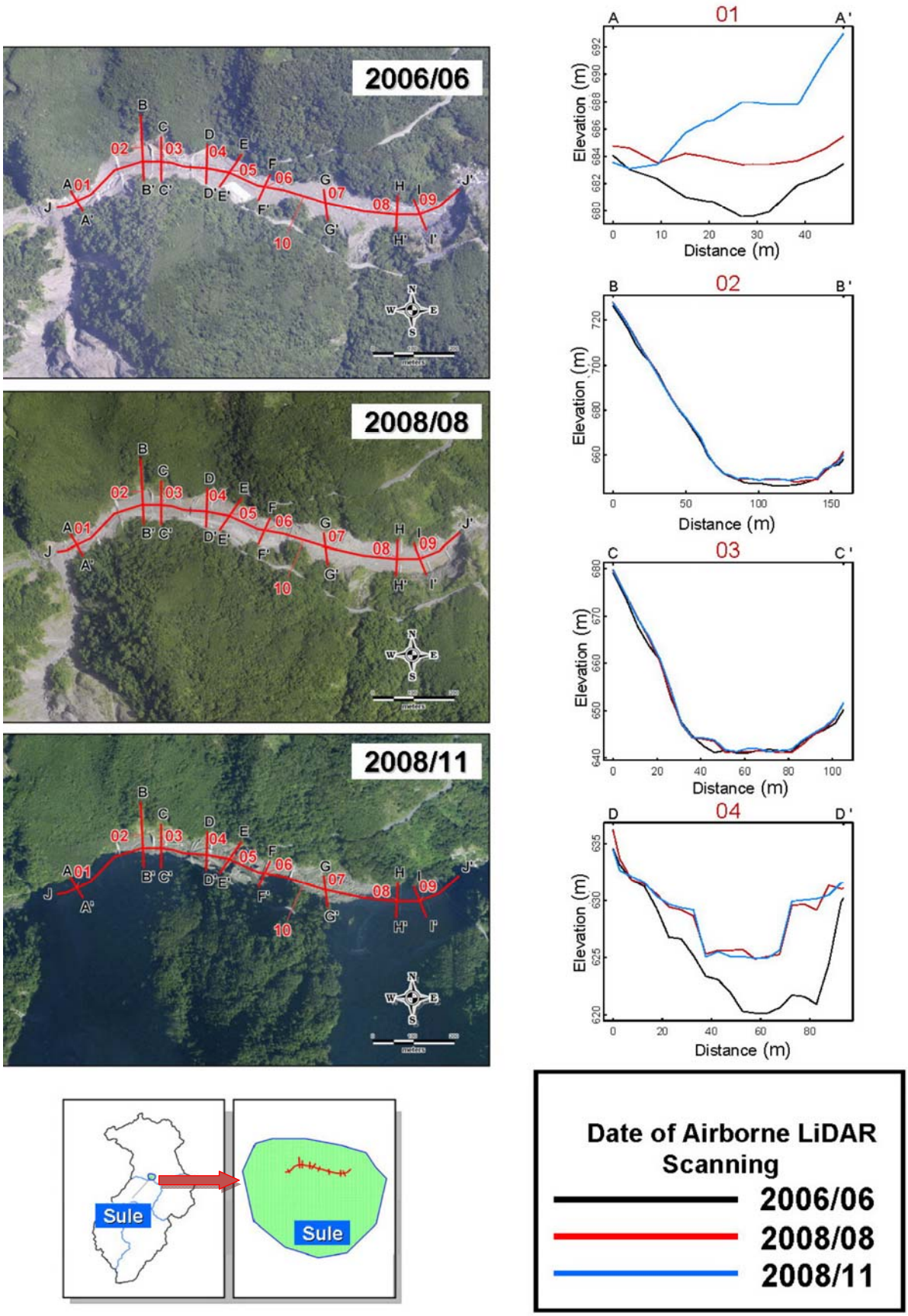

Fig. 24 Cross section analysis of Sule region

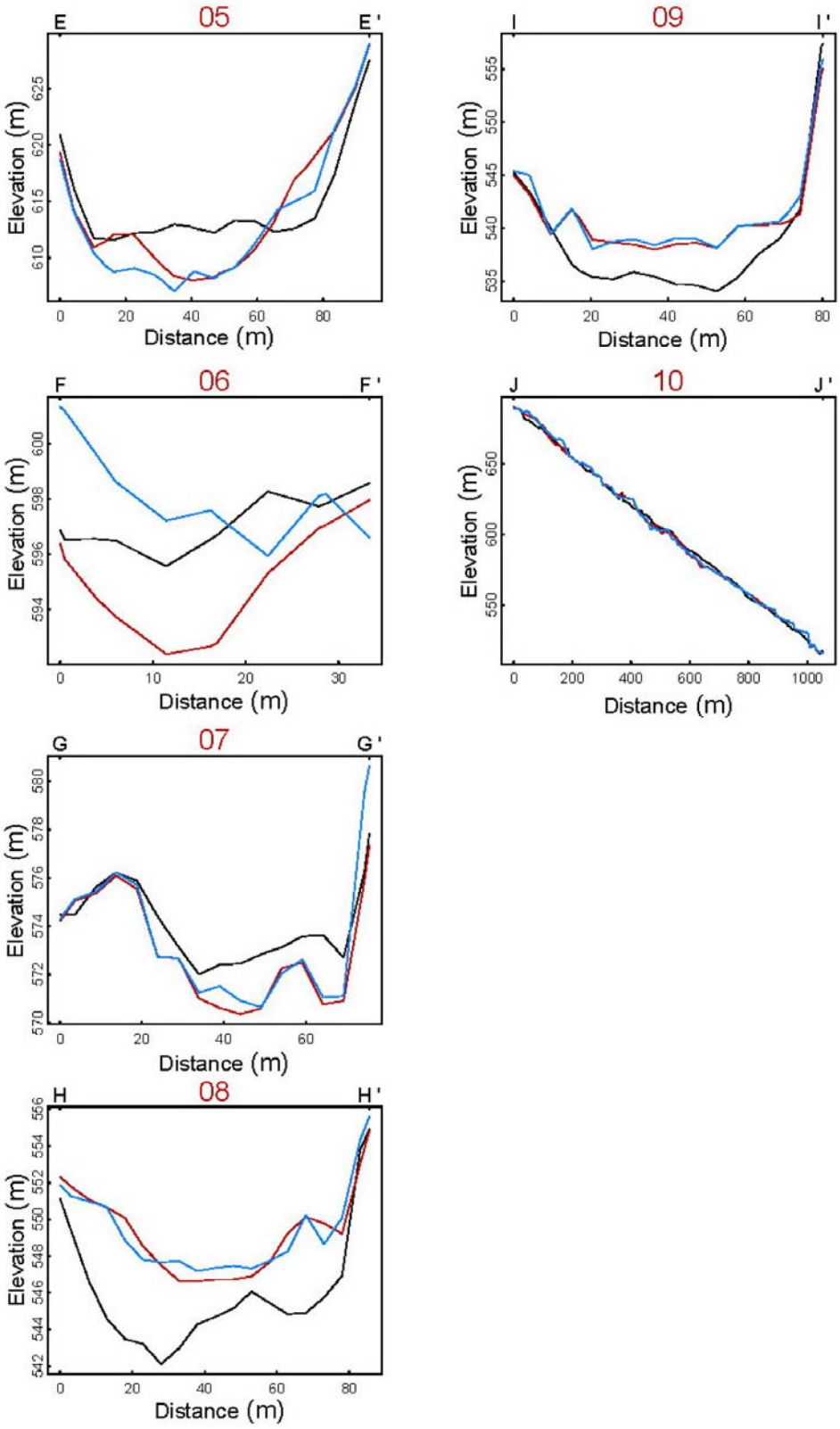

Fig. 24 (Continued)

Table 7 Variation of sediment yields in remediation region

Remediation region	Variation of sediment yields (m^3) 2006.06 ~ 2008.08	Variation of sediment yields (m^3) 2008.08 ~ 2008.11
Hsiawenkuang	38,587.0	4,098.7
Taiping	19,160.2	3,459.8
Shaluntsai	8,316.1	5,352.1
Sule	132,640.2	9,426.5
Paoliku	9,138.8	804.2
Junghua	10,121.7	3,008.8
Yihsing	N/A	2,024.6
Total	217,964.0	28,174.7

6. CONCLUSIONS

A series of DEMs, produced by airborne LiDAR during different periods, were analysed and the effectiveness of the hillslope and waterway remediation efforts confirmed. High-precision DEM may be used to monitor sediment movement and identify sediment production sources. According to the results of Variation of Sediment Yields, after completion of Vegetation restoration and slope remediation projects in 2008, the overall remediation at these priority remediation regions was effective. However several large sediment disasters should continue to be monitored and remediated. Hence, LiDAR should be applied for periodic monitoring of disaster-prone areas. High-precision and high-resolution three dimensional terrain data were completed using remote sensing and other geographical information data sets to identify disaster areas, analyse topological changes and erosion and deposit areas.

Upstream watershed conservation efforts were used to reduce sediment deposition into the reservoir and increase its lifespan. This increases the sustainability of the reservoir by stabilizing sediment yields and reducing sediment discharges in the reservoir. In response to the recent extreme hydrological activities and climate changes, it is recommended that involved governmental agencies conduct comprehensive watershed check-ups and establish relevant databases through disaster-prevention monitoring or multi-scale telemetry. Such actions will assist in understanding sediment yield as well as the process of its movement.

ACKNOWLEDGEMENTS

This work is a partial result of the studies funded by research contract SWCB-98-007, Soil and Water Conservation Bureau, ROC. The authors express their sincere gratitude for the support.

REFERENCES

Abellán, A., Jaboyedoff, M., Oppikofer, T., and Vilaplana, J. M. (2009). "Detection of millmetric deformation using a terrestrial laser scanner: Experiment and application to a rockfall event." *Natural Hazards and Earth System Sciences*, **9**, 365–372.

Avian, M., Kellerer-Pirklbauer, A., and Bauer, A. (2009). "LiDAR for monitoring mass movements in Permafrost environments at the Cirque Hinteres Langtal, Austria, between 2000 and 2008." *Natural Hazards and Earth System Sciences*, **9**, 1087–1094.

Croke, J., Todd, P., Thompson, C., Watson, F., Denham, R., and Khanal, G. (2013). "The use ofmulti temporal LiDAR to assess basin-scale erosion and deposition following the catastrophic January 2011 Lockyer flood, SE Queensland, Australia." *Geomorphology*, **184**, 111–126.

Evans, J.S., Hudak, A.T., Faux, R., and Smith, A.M.S. (2009). "Discrete return LiDAR in natural resources: Recommendations for project planning, data processing, and deliverables." *Remote Sensing*, **1**, 776–794.

Hsiao, C.Y., Hsieh, P.S., and Chi, S.Y. (2011). "Assessing volume earthwork by using unconventional photogrametry." *Proceedings of the Second World Landslide Forum*, Rome, 3–7.

Jaboyedoff, M., Oppikofer, T., Abellán, A., Derron, M.H., Loye, A., Metzger R., and Pedrazzini, A. (2012). "Use of LiDAR in landslide investigations: A review." *Natural Hazards*, **61**(1), 5–28.

Leica Geosystems (2003). ALS50 Airborne Laser Scanner, Leica Geosystems, URL: http://gis.leica-geosystems.com/.

Lin, B.S. (2010). "Estimation of sediment discharge and trapping efficiency in Shihmen watershed from LiDAR technology." *The Young Southeast Asia Geotechnical Conference*, Taipei, Taiwan, 9–12.

Lin, B.S, Hsiao, C.Y., Leung, W.Y., and Chi, S.Y. (2012a). "Using airborne LiDAR technology to analyze landslide hazards in Shihmen watershed." *European Geosciences Union*, General Assembly 2012, 14, EGU2012-2884, Vienna, Austria, 22–27.

Lin, B.S., Chen, C.K, Hsiao, C.Y., and Chi, S.Y. (2012b). "Using multi-scale monitoring technology with airborne LiDAR DEMs to evaluate remediation efficiency of sediment disaster in Shih-

men reservoir watershed." *The 5th Taiwan-Japan Joint Workshop on Geotechnical Hazards from Large Earthquakes and Heavy Rainfall*, SVI-7.

Lin, B.S., Ho, H.C., Hsiao, C.Y., Jeff, K., Chen, C.K., and Chi, S.Y. (2013). "Using multi-scale sediment monitoring techniques to evaluate remediation effectiveness of the Tsengwen reservoir watershed after sediment disasters induced by typhoon Morakot." *Proceedings of the 18th International Conference for Soil Mechanics and Geotechnical Engineering*, Paris, France, 571–574.

Schenk, T. (2001). "Modeling and analyzing systematic errors in airborne laser scanners." Technical Report in Photogrammetry, 19, Ohio State University.

Shih, T.Y., Peng, M.H., and Hsu, W.C. (2002). "Mapping earthquake hazard with airborne LiDAR system." Research Report, Taiwan Council of Agriculture (in Chinese).

Sinotech Engineering Consultants (2006). *A Study on Investigation and Countermeasure Strategy of Landslide and Potential Debris Flows from Te-Chi Watershed to Ma-An Dam in Da-Chia River Basin*, Taiwan Power Company (in Chinese).

Sithole, G. and Vosselman, G. (2004). "Experimental comparison of filter algorithms for bare-earth extraction from airborne laser scanning point clouds." *ISPRS Journal of Photogrammetry and Remote Sensing*, **59**(1-2), 85–101.

Soil Water Conservation Bureau (SWCB) (2006). *Technical Regulations for Soil and Water Conservation* (in Chinese).

Soil Water Conservation Bureau (SWCB) (2009). *Study on High Quality Measurement and Terrain Historical Migration in Shihmen Watershed*, SWCB-98-007 (in Chinese).

Soil Water Conservation Bureau (SWCB) (2010). *Study on Historical Migration and Its Mechanism of Heavy Rainfall-Induced Sediment Disaster in Shihmen Watershed*, SWCB-99-005 (in Chinese).

Sturzenegger, M. and Stead, D. (2009). "Quantifying discontinuity qrientation and persistence on high mountain rock slopes and large landslides using terrestrial remote sensing techniques." *Natural Hazards and Earth System Sciences*, **9**, 267–287.

Tarchi, D., Casagli, N., Fanti, R., Leva, D.D., Luzi, G., Pasuto, A., Pieraccini, M., and Silvano, S. (2003). "Landslide monitoring by using ground-based SAR interferometry: An example of application to the Tessina landslide in Italy." *Engineering Geology*, **68**, 15–30.

Yang, L. Y. (2007). "Coastal morphological change of south Dansuie River Estuary, North Taiwan." Master Thesis, Department of Geography, National Taiwan University (in Chinese).